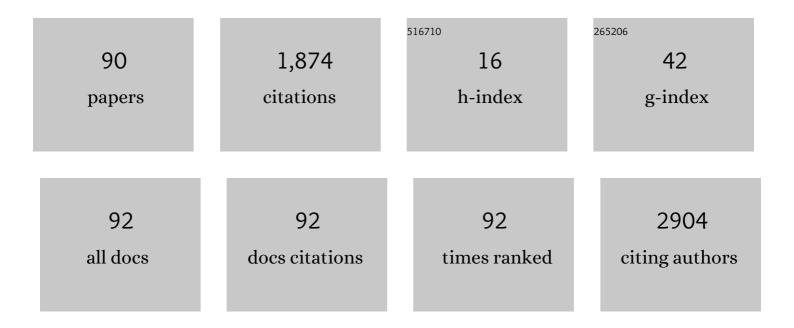
Roberto dos Reis

List of Publications by Year in descending order

Source: https://exaly.com/author-pdf/5272883/publications.pdf Version: 2024-02-01



#	Article	IF	CITATIONS
1	Enhanced ferroelectricity in ultrathin films grown directly on silicon. Nature, 2020, 580, 478-482.	27.8	486
2	Conductive 2D metal-organic framework for high-performance cathodes in aqueous rechargeable zinc batteries. Nature Communications, 2019, 10, 4948.	12.8	398
3	Improved Subthreshold Swing and Short Channel Effect in FDSOI n-Channel Negative Capacitance Field Effect Transistors. IEEE Electron Device Letters, 2018, 39, 300-303.	3.9	128
4	Synthesis and Characterisation of Fluorescent Carbon Nanodots Produced in Ionic Liquids by Laser Ablation. Chemistry - A European Journal, 2016, 22, 138-143.	3.3	75
5	Dependence of random laser emission on silver nanoparticle density in PMMA films containing rhodamine 6G. Journal of the Optical Society of America B: Optical Physics, 2011, 28, 1118.	2.1	60
6	Self-Assembly of Two-Dimensional Perovskite Nanosheet Building Blocks into Ordered Ruddlesden–Popper Perovskite Phase. Journal of the American Chemical Society, 2019, 141, 13028-13032.	13.7	59
7	Stabilization of ferroelectric phase in tungsten capped Hf0.8Zr0.2O2. Applied Physics Letters, 2017, 111, .	3.3	58
8	Crystalline Molybdenum Oxide Thin-Films for Application as Interfacial Layers in Optoelectronic Devices. ACS Applied Materials & Interfaces, 2017, 9, 7717-7724.	8.0	44
9	Determination of the structural phase and octahedral rotation angle in halide perovskites. Applied Physics Letters, 2018, 112, .	3.3	38
10	Electronic band structure of ZnO-rich highly mismatched ZnO1â^'xTex alloys. Applied Physics Letters, 2015, 106, .	3.3	27
11	Mapping Grains, Boundaries, and Defects in 2D Covalent Organic Framework Thin Films. Chemistry of Materials, 2021, 33, 1341-1352.	6.7	25
12	Room-Temperature-Synthesized High-Mobility Transparent Amorphous CdO–Ga ₂ O ₃ Alloys with Widely Tunable Electronic Bands. ACS Applied Materials & Interfaces, 2018, 10, 7239-7247.	8.0	24
13	Direct Visualization of Electric-Field-Induced Structural Dynamics in Monolayer Transition Metal Dichalcogenides. ACS Nano, 2020, 14, 1569-1576.	14.6	23
14	Persistent luminescence of inorganic nanophosphors prepared by wet-chemical synthesis. Journal of Alloys and Compounds, 2018, 732, 705-715.	5.5	21
15	Interpretable and Efficient Interferometric Contrast in Scanning Transmission Electron Microscopy with a Diffraction-Grating Beam Splitter. Physical Review Applied, 2018, 10, .	3.8	20
16	Oriented LiMn ₂ O ₄ Particle Fracture from Delithiation-Driven Surface Stress. ACS Applied Materials & Interfaces, 2020, 12, 49182-49191.	8.0	20
17	OHM Sponge: A Versatile, Efficient, and Ecofriendly Environmental Remediation Platform. Industrial & Engineering Chemistry Research, 2020, 59, 10945-10954.	3.7	18
18	P ₂ S ₅ Reactive Flux Method for the Rapid Synthesis of Mono- and Bimetallic 2D Thiophosphates M _{2–<i>x</i>} M′ _{<i>x</i>} P ₂ S ₆ . Inorganic Chemistry, 2021, 60, 3502-3513.	4.0	18

#	Article	IF	CITATIONS
19	Degeneration Behavior of Cu Nanowires under Carbon Dioxide Environment: An <i>In Situ</i> / <i>Operando</i> Study. Nano Letters, 2021, 21, 6813-6819.	9.1	18
20	Growth and transport properties of p-type GaNBi alloys. Journal of Materials Research, 2011, 26, 2887-2894.	2.6	16
21	Spatial Mapping of Hotâ€5pots at Lateral Heterogeneities in Monolayer Transition Metal Dichalcogenides. Advanced Materials, 2019, 31, 1808244.	21.0	16
22	Work function mapping of MoOx thin-films for application in electronic devices. Ultramicroscopy, 2017, 183, 99-103.	1.9	15
23	Blue–green luminescent carbon nanodots produced in a silica matrix. Carbon, 2015, 91, 234-240.	10.3	14
24	Topology of transition metal dichalcogenides: the case of the core–shell architecture. Nanoscale, 2020, 12, 23897-23919.	5.6	14
25	Raman and TEM characterization of high fluence C implanted nanometric Si on insulator. Applied Surface Science, 2012, 258, 7395-7400.	6.1	13
26	Making the most of your electrons: Challenges and opportunities in characterizing hybrid interfaces with STEM. Materials Today, 2021, 50, 100-115.	14.2	13
27	Structural changes of potassium-saturated smectite at high pressures and high temperatures: Application for subduction zones. Applied Clay Science, 2014, 102, 164-171.	5.2	12
28	Phosphate Elimination and Recovery Lightweight (PEARL) membrane: A sustainable environmental remediation approach. Proceedings of the National Academy of Sciences of the United States of America, 2021, 118, .	7.1	12
29	Molecular beam epitaxy of GaN _{1–<i>x</i>} Bi _{<i>x</i>} alloys with high bismuth content. Physica Status Solidi (A) Applications and Materials Science, 2012, 209, 419-423.	1.8	11
30	Antiferromagnetic Semiconductor BaFMn _{0.5} Te with Unique Mn Ordering and Red Photoluminescence. Journal of the American Chemical Society, 2019, 141, 17421-17430.	13.7	10
31	Uncovering the crystal defects within aragonite CaCO ₃ . Proceedings of the National Academy of Sciences of the United States of America, 2022, 119, e2122218119.	7.1	10
32	Formation of Nanoscale Composites of Compound Semiconductors Driven by Charge Transfer. Nano Letters, 2016, 16, 5247-5254.	9.1	9
33	Ion beam synthesis of cubic-SiC layer on Si(111) substrate. Journal of Applied Physics, 2006, 100, 063504.	2.5	8
34	Structural defects in transition metal dichalcogenide core-shell architectures. Applied Physics Letters, 2021, 118, .	3.3	8
35	Hidden Complexity in the Chemistry of Ammonolysis-Derived "Î ³ -Mo ₂ N― An Overlooked Oxynitride Hydride. Chemistry of Materials, 2021, 33, 6671-6684.	6.7	8
36	Mixed Metal Thiophosphate Fe _{2–<i>x</i>} Co _{<i>x</i>} P ₂ S ₆ : Role of Structural Evolution and Anisotropy. Inorganic Chemistry, 2021, 60, 17268-17275.	4.0	8

#	Article	IF	CITATIONS
37	Resonance Couplings in Si@MoS ₂ Core–Shell Architectures. Small, 2022, 18, e2200413.	10.0	8
38	Effects of the Encapsulation Membrane in Operando Scanning Transmission Electron Microscopy. Nano Letters, 2022, 22, 4137-4144.	9.1	8
39	Au@MoS ₂ @WS ₂ Core–Shell Architectures: Combining Vapor Phase and Solution-Based Approaches. Journal of Physical Chemistry C, 2020, 124, 2627-2633.	3.1	7
40	Influence of CO annealing in metal-oxide-semiconductor capacitors with SiO2 films thermally grown on Si and on SiC. Journal of Applied Physics, 2016, 119, .	2.5	6
41	Mechanism of non-catalytic chemical vapor deposition growth of all-inorganic CsPbX ₃ (X) Tj ETQq1 I	l 0.78431	4 ₆ gBT /Ove
42	Ion beam synthesis of SiC by C implantation into SIMOX(111). Nuclear Instruments & Methods in Physics Research B, 2009, 267, 1281-1284.	1.4	5
43	Microstructure of GaN1â^'x Bi x. Journal of Electronic Materials, 2013, 42, 26-32.	2.2	5
44	Passivation of defects in ZnO nanowires by SiO2 sputtering deposition. Materials Letters, 2014, 134, 126-129.	2.6	5
45	Structural defects in bulk GaN. Journal of Crystal Growth, 2014, 403, 66-71.	1.5	5
46	Doping of GaN1â^'xAsx with high As content. Journal of Applied Physics, 2011, 110, 093702.	2.5	4
47	Synthesis, Characterization, and Simulation of Four-Armed Megamolecules. Biomacromolecules, 2021, 22, 2363-2372.	5.4	4
48	Nanoscale Investigation of Layered Oxychloride Intergrowth Photocatalysts for Visible Light Driven Water Splitting. Microscopy and Microanalysis, 2020, 26, 376-379.	0.4	4
49	Perovskite-like K ₃ TiOF ₅ Exhibits (3 + 1)-Dimensional Commensurate Structure Induced by Octahedrally Coordinated Potassium Ions. Journal of the American Chemical Society, 2021, 143, 18907-18916.	13.7	4
50	Carbon redistribution in nanometric Si1â^'xCxlayers upon ion beam synthesis of SiC by C implantation into SIMOX(1 1 1). Journal Physics D: Applied Physics, 2010, 43, 395401.	2.8	3
51	Towards Identification of Oxygen Point Defects by Means of Position Averaged CBED. Microscopy and Microanalysis, 2015, 21, 1097-1098.	0.4	3
52	The importance of structural inhomogeneity in GaN thin films. Journal of Crystal Growth, 2016, 456, 160-167.	1.5	3
53	Photoluminescence properties of arsenic and boron doped Si ₃ N ₄ nanocrystal embedded in SiN _{<i>x</i>} O _{<i>y</i>} matrix. Materials Research Express, 2018, 5, 036201.	1.6	3
54	Probing single-unit-cell resolved electronic structure modulations in oxide superlattices with standing-wave photoemission. Physical Review B, 2019, 100, .	3.2	3

#	Article	IF	CITATIONS
55	Selective suppression of {112} anatase facets by fluorination for enhanced TiO ₂ particle size and phase stability at elevated temperatures. Nanoscale Advances, 2021, 3, 6223-6230.	4.6	3
56	Towards Quantum Image Processing for Electron Microscopy. Microscopy and Microanalysis, 2021, 27, 1348-1351.	0.4	3
57	Structural Characterization of Si1-xCx Nanolayers Synthesized by C Implantation into SiO2/Si. ECS Transactions, 2011, 39, 95-101.	0.5	2
58	Direct atomic imaging of antiphase boundaries and orthotwins in orientation-patterned GaAs. Applied Physics Letters, 2013, 102, 081905.	3.3	2
59	Photoluminescence from doped silicon nanocrystals in SiO <inf>2</inf> matrix. , 2013, , .		2
60	The influence of the substrate misorientation on the structural quality of GaN layers grown by HVPE. Journal of Crystal Growth, 2018, 498, 346-351.	1.5	2
61	Spatial Mapping of Electrostatic Fields in 2D Heterostructures. Nano Letters, 2021, 21, 7131-7137.	9.1	2
62	Photoluminescence Emission from Si Nanocrystals in SiO ₂ Matrix Obtained by Reactive Sputtering. Advanced Science, Engineering and Medicine, 2014, 6, 277-282.	0.3	2
63	Probing the Optical Response and Local Dielectric Function of an Unconventional Si@MoS ₂ Core–Shell Architecture. Nano Letters, 2022, 22, 4848-4853.	9.1	2
64	Wurtzite-to Amorphous-to Cubic Phase Transition of GaN _{1-X} As _x Alloys with Increasing as Content. Solid State Phenomena, 0, 186, 74-77.	0.3	1
65	Structural studies of GaN _{1â€x} As _x and GaN _{1â€x} Bi _x alloys for solar cell applications. Physica Status Solidi C: Current Topics in Solid State Physics, 2012, 9, 1586-1589.	0.8	1
66	Microstructure of Mg doped GaNAs alloys. Physica Status Solidi C: Current Topics in Solid State Physics, 2013, 10, 453-456.	0.8	1
67	Revealing Point Defects in a Large-Scale Scanning Diffraction Dataset. Microscopy and Microanalysis, 2016, 22, 470-471.	0.4	1
68	Multimodal Characterization of the Oleophilic Hydrophobic Magnetic (OHM) Sponge: <i>A Nanocomposite Material for Oil Spill Remediation</i> . Microscopy and Microanalysis, 2020, 26, 2754-2756.	0.4	1
69	Structural and chemical analysis of mixed cation antiferromagnetic layered metal chalcophosphate FeCoP2S6. Microscopy and Microanalysis, 2021, 27, 140-143.	0.4	1
70	Show me your "Hand― Direct determination of "handedness―in NaCu ₅ S ₃ chiral crystal via aberration-corrected scanning transmission electron microscopy. Microscopy and Microanalysis, 2021, 27, 2652-2654.	0.4	1
71	Planar defects in patterned GaAs by aberration corrected STEM. Microscopy and Microanalysis, 2012, 18, 338-339.	0.4	0
72	Ne–He bubble formation in co-implanted Si(111) substrates. Thin Solid Films, 2013, 548, 465-469.	1.8	0

#	Article	IF	CITATIONS
73	Reply. Journal of Cataract and Refractive Surgery, 2019, 45, 890-891.	1.5	0
74	Electronic Biasing of Monolayer Transition Metal Dichalcogenides in a TEM. Microscopy and Microanalysis, 2019, 25, 1904-1905.	0.4	0
75	Identification of Anion Sites in BiCuXO (X= Se, S) Heteroanionic Materials. Microscopy and Microanalysis, 2019, 25, 2106-2107.	0.4	0
76	Revealing the Complex Structural Intergrowth Within Ternary W-Nb-O Oxide. Microscopy and Microanalysis, 2019, 25, 2172-2173.	0.4	0
77	Emerging Opportunities in STEM to Characterize Soft-Hard Interfaces. Microscopy and Microanalysis, 2021, 27, 616-618.	0.4	0
78	Soft Microscopy of Negative Stained Soft Materials: Balancing Dose Rate and Sample Damage. Microscopy and Microanalysis, 2021, 27, 1408-1411.	0.4	0
79	Exploring the inner space of outer space: multi-length scale, multimodal characterization of Muonionalusta IVA iron meteorite. Microscopy and Microanalysis, 2021, 27, 2264-2266.	0.4	0
80	Multimodal Characterization of Hierarchically Porous Nanocomposite Materials: The Case Study of the PEARL Membrane. Microscopy and Microanalysis, 2021, 27, 2006-2009.	0.4	0
81	To Cryo or Not to Cryo? A Consideration of Length Scales During Macromolecule Sample Preparation. Microscopy and Microanalysis, 2021, 27, 1404-1407.	0.4	0
82	Leveraging Hybrid Pixel Electron Detection Technology to Expand Electron Microscopy Observation of Material Structures at low Voltages. Microscopy and Microanalysis, 2021, 27, 1000-1002.	0.4	0
83	Spatial Mapping of Electrostatics and Dynamics in Quantum Materials. Microscopy and Microanalysis, 2021, 27, 1436-1438.	0.4	0
84	Phase Retrieval Imaging for Soft Materials at Low-Voltage. Microscopy and Microanalysis, 2021, 27, 1826-1828.	0.4	0
85	Si@MoS2 Core-Shell Architecture: Characterizations and Implications for Nanophotonic Applications. Microscopy and Microanalysis, 2021, 27, 650-652.	0.4	0
86	Simultaneous imaging of light and heavy elements at atomic resolution using electron ptychography and fast pixelated detectors. Acta Crystallographica Section A: Foundations and Advances, 2017, 73, a168-a168.	0.1	0
87	Symmetry group determination and direct imaging of all-inorganic halide perovskites CsPbBr3â^'x Cl x. Acta Crystallographica Section A: Foundations and Advances, 2017, 73, a217-a217.	0.1	0
88	Electron ptychographic phase imaging using fast pixelated detectors. Acta Crystallographica Section A: Foundations and Advances, 2017, 73, C1349-C1349.	0.1	0
89	Quantitative determination of polarization from 4D scanning electron diffraction experiments. Acta Crystallographica Section A: Foundations and Advances, 2018, 74, a327-a327.	0.1	0
90	Probing properties and structure of complex oxides superlattices using scanning electron nanodiffraction. Acta Crystallographica Section A: Foundations and Advances, 2018, 74, a392-a392.	0.1	0